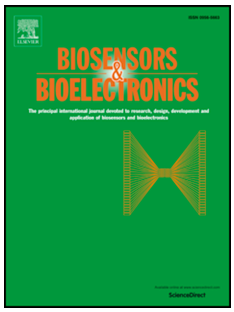

Distance-dependent plasmon-enhanced electrochemiluminescence biosensor based on MoS_2 nanosheets

Yang Liu, Yixin Nie, Mengke Wang, Qian Zhang, Qiang Ma

PII: S0956-5663(19)30902-9

DOI: https://doi.org/10.1016/j.bios.2019.111823

Reference: BIOS 111823

To appear in: *Biosensors and Bioelectronics*

Received Date: 11 September 2019

Revised Date: 20 October 2019

Accepted Date: 24 October 2019

Please cite this article as: Liu, Y., Nie, Y., Wang, M., Zhang, Q., Ma, Q., Distance-dependent plasmon-enhanced electrochemiluminescence biosensor based on MoS_2 nanosheets, *Biosensors and Bioelectronics* (2019), doi: https://doi.org/10.1016/j.bios.2019.111823.

Distance-dependent Plasmon-Enhanced Electrochemiluminescence Biosensor based on MoS_2 nanosheets

Yang Liu[a,b], Yixin Nie[a], Mengke Wang[a], Qian Zhang[a] and Qiang Ma[a]*

[a] *Department of Analytical Chemistry, College of Chemistry, Jilin University, Changchun, 130012, China*

[b] *Electron Microscopy Center, Jilin University, Changchun, 130012, China*

*Corresponding author

Tel.: +86-431-85168352

E-mail address: *Qma@jlu.edu.cn*

Abstract

Nonmetallic plasmonic MoS_2 nanosheets were synthesized by hydrothermal top-down method. MoS_2 nanosheets had shown strong surface plasmon coupling (SPC) light absorption in the visible and near-infrared region. Herein, the nonmetallic plasmonic MoS_2 nanosheets were employed to enhance the electrochemiluminescence (ECL) signal of sulfur doped boron nitrogen QDs (S-BN QDs) in this work. It is important to regulate the distance between ECL luminophore and plasmonic nanoparticles. On one hand, too closed distance can cause energy or electron transfer, which could quench the ECL intensity of nano-luminophore. On the other hand, plasmonic nanostructure cannot significantly affect the luminescence in the far distance. Therefore, we discussed the distance-dependent plasmon-enhanced ECL in detail with different length DNA chains. Furthermore, we constructed a hybridization chain reaction (HCR) amplification ECL sensing mode with the SPC-ECL strategy. The proposed DNA sensor can quantify hepatitis C virus (HCV) gene from 0.5 pmol/L to 1 nmol/L with a limit of detection (LOD) of 0.17 pmol/L.

Keywords: MoS_2 nanosheets, surface plasmon coupling ECL, ECL-energy resonance transfer, biosensor, HCV gene, distance-dependent sensing,

Introduction

Hepatitis C virus (HCV) was single-stranded virus. HCV have been proved to be the most common case of hepatitis in the world. In addition, about 200 million people worldwide suffer from chronic hepatitis and about 1 million die from chronic viral hepatitis. Furthermore, the infection rate of HCV is increasing in China (Weinbaum et al., 2009; Welzel et al., 2017; Hrift et al., 2017). Long-time chronic hepatitis can eventually lead to serious liver diseases such as cirrhosis and hepatocellular carcinoma (HCC) (Brody et al., 2011). HCV infection remains a serious health problem worldwide. Therefore, early diagnosis of chronic hepatitis plays an important role in hepatitis and some liver diseases, and can effectively control the spread of the disease (Welzel et al., 2017; Eguchi et al., 2014). Therefore, some detection methods have been developed for HCV, including ELISA, fluorescence detection. Despite these methods display excellent sensitivity and selectivity, time-consuming and simple operation is required. Thus, it is still essential to develop a simple and rapid method for the detection of HCV gene.

Electrochemiluminescence (ECL) detection for biosensing and medical examination has the characteristics of simple equipment, fast response, high sensitivity, good reproducibility and low background noise (Li et al., 2017; Miao et al., 2008; Qing et al., 2017; Richter et al., 2004; Delaney et al., 2011; Jiang et al., 2007). Recently, ECL technology has been widely used in biosensor construction. Zhu et al. has designed a sandwich-type immunosensor based ECL-RET to detect prostate specific antigen (PSA) (Zhu et al., 2018). Ge et al. has constructed a paper-based closed bipolar electrode (BPE) ECL biosensor to detect human breast cancer cells (MCF-7) (Ge et al., 2018). Nie et al. has designed an ECL signal amplification strategy based onP5FIn/erGO to detect carcinoembryonic antigen (CEA) (Nie et al., 2018). Peng et al. has based quenching effect of ferrocene-labeled DNA (Fc-DNA) to design an ECL biosensor to detect miRNA-21 (Peng et al., 2019). ECL is an electrically generated light emission process, which includes the excited state luminescence of the luminophores due to the initial electrochemical reaction on the

electrode surface (Piriaud et al., 2013). The most traditional ECL luminescence was ruthenium(II)tris(2,2-bipyridyl) ($Ru(bpy)_3^{2+}$) and it attracted many attentions because of its high luminescence efficiency and chemical stability (Ege et al., 1984). Since the Si quantum dots (QDs) were reported in 2002, QDs as a new type of ECL luminescence have been developed (Ding et al., 2002). However, ECL luminophore, especially QDs and other nanoparticles, suffers from the defect of low brightness, which limits the potential ECL sensing applications (Xu et al., 2014). So, during the fabrication of ECL biosensors, enhancement of the luminous efficiency is vital for the biological detection (Liu et al., 2015). So, the ECL enhancement based on plasma nanoparticles attracted more and more attention (Liu et al., 2019; Liu et al., 2018).

When two nanoparticles are close to each other, a single plasmon exciton is coupled to form dimers (Weller et al., 2016), which results in localized surface plasmons transfer in extinction spectrum (Halas et al., 2011; Qian et al., 2017) and electromagnetic field enhancement (Kessentini et al., 2014; Shao et al., 2010). The integration of semiconductor nanomaterials and metal nanoparticles realized light emission modulation by surface plasmons and provides the opportunity to modify the emission response of nanomaterials through the interaction between the external magnetic field and surface plasmons (Shan et al., 2016). Localized surface plasmons have been used not only in surface Raman spectroscopy, but also in the field of the plasmon-enhanced fluorescence and ECL. It provided a pathway to overcome the intrinsic defects of low emission intensities form the nano-fluorescence or ECL luminophore (e,g, QDs, NIR dyes, and up-conversion luminescent material). The surface plasmon coupling ECL phenomenon was caused by the resonant interaction of the light with the electron oscillations in the metal (Zhang et al., 2004; Deiss et al., 2009; Aslan et al., 2009; Lakouwicz et al., 2008). Until now, there are still two problems in the plasmon-enhanced ECL research. Firstly, most plasmonic nanostructures are based on the noble metals (Au, Ag, and Pt). The surface plasmon coupling characteristics were closely related to material carrier concentration. Only a sufficiently high carrier concentration on the noble metals can generate strong surface plasmon resonance in the corresponding wave band. But the low storage and high cost

of these noble metals limited the practical application in plasmon-enhanced ECL sensors. Secondly, the distance between luminophore and plasmonic nanoparticles played a key role in the ECL sensing process. Almost plasmonic nanoparticles can also work as energy or electron acceptor, which have the strong quenching ability. So, when the luminophore is closed to plasmonic nanoparticles, the ECL signal could be quenched easily instead of the enhancement. Many ECL sensors use DNA or adaptors to control the distance between the luminescence and the nanoparticles to achieve ECL-resonant energy transfer (ECL-RET) or surface plasma coupling-ECL (SPC-ECL). Gai et al. has designed a distance-dependent DNA sensor through the opening and closing of hairpin DNA, realizing ECL-RET and SPC-ECL effects between Au NPs and $Ru(bpy)_3^{2+}$ (Gai et al., 2018). Feng et al. realized the enhancement of the localized surface plasmon resonance-ECL (LSPR-ECL) of Ag NCs by using the catalytical hairpin assembly amplification (CHA) technology to design a sensor that regulated the distance between Au NPs and Ag NCs through DNA (Feng et al., 2019). Lu et al. has achieved ECL-RET effect of Au nanocages on Rusi NPs by tetrahedron DNA and hairpin DNA (Lu et al., 2018).

In recent years, some low-cost non-metallic materials (metal oxides/sulfides) with SPC phenomenon have attracted attention as potential substitutes for plasma precious metals. The free carrier density on metal oxides/sulfides can be improved by heavy doping. As a kind of low-cost non-metallic materials, self-doped semiconductors such as WO_{3-x} (Lou et al., 2015; Lou et al., 2016; Ishii et al., 2018), MoO_{3-x} (Kuwahara et al., 2018; Cheng et al., 2016), $Cu_{2-x}S$ (Wang et al., 2015; Alam et al., 2016), and MoS_2 nanosheets had the advantages of easy synthesis and surface plasmons effect in the visible light and near infrared region, and have been applied to catalysis and tumor therapy based on the plasma thermal effect (Kaur et al., 2018, Huang et al., 2015; Zhu et al., 2017; Wen et al., 2016). Sulfur doped BN QDs with high electro-optic activity and good ECL properties were employed as ECL luminophore in this work. As shown in Scheme 1, we discussed the distance relation between MoS_2 nanosheets plasmonic effects and the ECL luminescence of sulfur doped boron nitrogen QDs (S-BN QDs). And the hybridization chain reaction (HCR)

sensing process was employed to sensitively detect target HCV gene. HCR is a simple and efficient isothermal enzyme-free DNA amplification method. HCR can effectively avoid unstable enzyme activity in other detection methods, harsh experimental conditions and other factors. HCR was a triggered self-assembly and enzyme-free process (Dirks et al., 2004). The technique can realize cascade hybridization events with high amplification ability, and eventually form long double-stranded DNA (dsDNA).

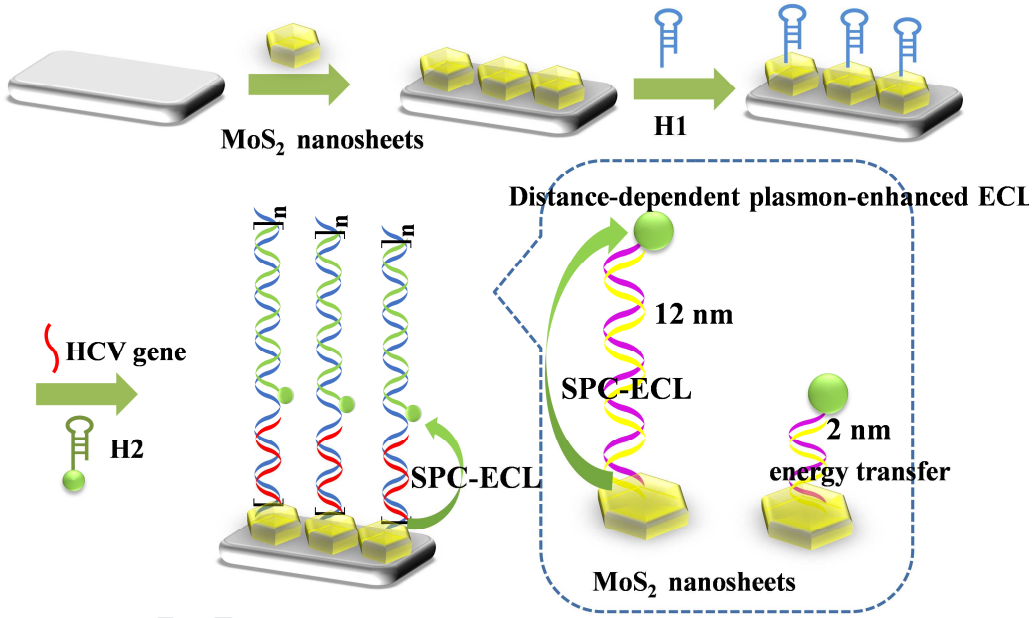

Scheme 1. The HCR-based sensing process and distance-dependent plasmon-enhanced ECL

2. Experiment Section

2.1 Materials

Boric acid (H_3BO_3), melamine ($C_3H_6N_6$), L-cysteine ($C_3H_7NO_2S$), sodium dihydrogen phosphate (NaH_2PO_4), disodium hydrogen phosphate (Na_2HPO_4) and sodium phosphate (Na_3PO_4) were purchased from Sigma Co. (Shanghai, China). Ammonium molybdate $(NH_4)_6Mo_7O_{24} \cdot 4H_2O$, thiourea, and Nethyl-N‘-(3-dimethylaminopropyl) carbodiimide hydrochloride (EDC), N-hydroxysulfosuccinimide (NHS) were obtained from Sinopharm Chemical Reagent Co.Ltd. The oligonucleotides used were synthesized and purified by Qingke Co., Ltd.

(Tianjin, China) (Table S1). All reagent solutions were prepared using ultrapure water (resistivity as 18 MΩ cm-1 at 25^{o}C). Human serum samples were obtained from the China-Japan union hospital of Jilin university.

2.2 Apparatus

TEM images of the nanomaterials were obtained with a Hitachi electron microscope operating at 200 kV acceleration voltages. FT-IR, Photoluminescence (PL), and UV–vis absorption spectra were acquired by Thermo Nicolet 360 FTIR spectrometer, Shimadzu RF-5301 PC spectrofluorophotometer and Hitachi UH5300 UV–vis spectrometer, respectively. The CV and EIS data were acquired with a CHI 660B electrochemical workstation with the glassy carbon electrode (GCE) as the working electrode. In the all electrochemical analysis process, a platinum wire and an Ag/AgCl (saturated KCl) electrode was employed as the counter electrode and the reference electrode, respectively.

2.3 Synthesis of MoS_2 nanosheets and S-BN QDs

MoS_2 nanosheets were synthesized by a hydrothermal method. 20 mg of ammonium molybdate and 40 mg of thiourea were dissolved in 12 mL of H_2O at room temperature. After the mixtures were stirred for 5 min, they were poured into a 20 mL Teflon-lined autoclave and subjected to heating at a temperature of 200 °C for 12 h, followed by natural cooling to room temperature.

The S-BN QDs were prepared according to our previous study (Liu et al., 2019). S-BN QDs were synthesized by a microwave-assisted hydrothermal method. Boric acid (1.6 mmol), melamine (0.27 mmol), and a certain amount of L-cysteine were dissolved in ultrapure water (10 mL). S-BN QDs were obtained under the 1000 Hz reflection frequency of microwave, 70 min and 120 ^{o}C. To remove excess precursors, the solution was centrifuged at 5000 rpm for 5 min and washed two times.

2.4 Synthesis of S-BN QDs -hairpin DNA2 (H2)

S-BN QDs and hairpin-DNA were connected by covalent link carboxyl and amino. 30 μL 10 mmol/L EDC and 10 μL 10 mmol/L NHS were added into

as-prepared 2 mL S-BN QDs to activate carboxyl of S-BN QDs with stirring for 15 min. Then, 15 μL 10 μmol/L H2 was added and stirred for 2 h. Finally, the solution was dialysed for 3 h to remove the unreacted small molecules.

2.5 ECL detection

Before ECL detection, GCE was polished with 1.0 and 0.05 μm Al_2O_3 powder, and then ultrasonically processed in ethanol and water respectively. GCE was immersed in PDDA solution to cover the surface of GCE with a PDDA film. Then 6 μL MoS_2 nanosheets and 10 μL hairpin DNA 1 (H1) were dropped on the PDDA/GCE, respectively. After reacting for 5 h at room temperature, the H1/ MoS_2 nanosheets/ PDDA/GCE electrode was dried under N_2 atmosphere. The above electrode was immersed with H2-QDs and different concentration of HCV gene for 2 h at 37^{o}C. Then, the electrode was dried under N_2 atmosphere. Finally, the ECL intensity of the resulting functionalized electrode was recorded in phosphate buffer solution (0.1 mol, pH 7.4) containing 0.1 M $K_2S_2O_8$ from -2 to 0V (versus Ag/AgCl) at the scan rate of 100 mV/s. The voltage of the photomultiplier tube (PMT) was set at 900 V in theprocess of detection.

3. Results and discussion

3.1 Characterizations of MoS_2 nanosheets and S-BN QDs

The morphology and microstructure of the MoS_2 nanosheets were shown in Fig 1 (A). The morphology and microstructure of the MoS_2 nanosheets were investigated by the field emission scanning electron microscope (TEM). MoS_2 nanosheets presented a regular sheet structure. Fig 1C displayed the XPS spectra of MoS_2 nanosheets, which showed that the MoS_2 nanosheets contained C, N, O, S, Mo elements. As shown in Fig S1A, the Mo 3d XPS spectrum exhibited two peaks at 233 eV and 236 eV, respectively. The two peaks corresponded to the Mo $3d_{5/2}$ and Mo $3d_{3/2}$ orbitals, respectively (Yu et al., 2015; Long et al., 2016; Xie et al., 2013). The two peaks at 163 eV and 168 eV of S 2p XPS spectrum (Fig S1B) corresponded to S $2p_{3/2}$ and S $2p_{1/2}$ orbitals, respectively, which was due to Mo-S bonding in MoS_2 nanosheets (Long et

al., 2016; Xie et al., 2013). And UV-vis spectrum showed the absorption peaks at 455 nm (Fig S3). As shown in Fig 1(B), S-BN QDs had uniform size distribution and the size of QDs was 7 nm. And the XPS spectra (Fig 1D) displayed that S-BN QDs contained C, N, O, B, S elements. UV-vis (Fig S2A) showed that the absorption peaks at 206 nm and 233 nm were attributed to n-σ* transitions in C-N bonds and π-π* transition of C=C bonds, respectively. FT-IR spectra (Fig S2B) can be used to characterize and identify chemical species. The peaks at 3195 cm^{-1} and 3338 cm^{-1} were due to the stretching vibration of O–H and N–H, which suggesting there were lots of amino and hydroxyl groups on the surface of S-BN QDs. The peaks were observed at 1184 cm^{-1}, 1575 cm^{-1} and 2373 cm^{-1}, which represented to –N-B-O-, -N=N= and S-H, respectively. And S-BN QDs also possessed the B-N stretching and B-N bending vibration peaks at 1280 cm^{-1} and 1575 cm^{-1}, respectively.

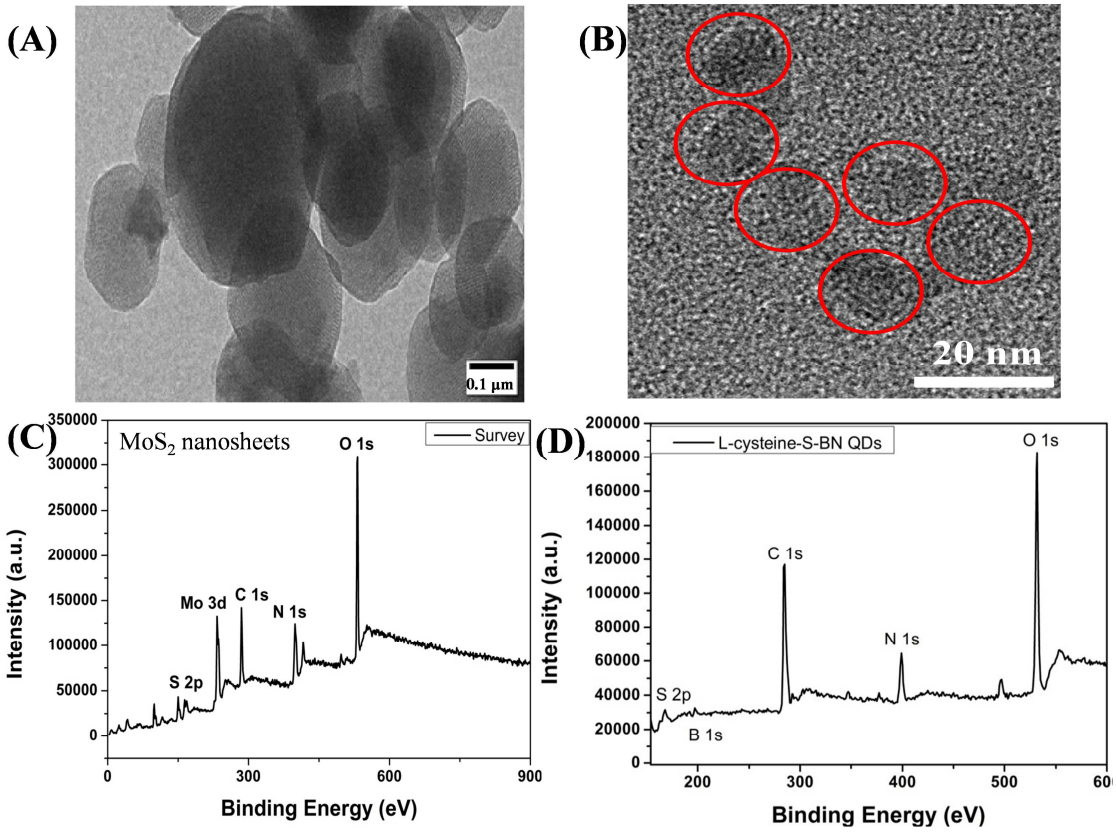

Fig 1. (A)&(B) TEM image of MoS_2 nanosheets and S-BN QDs. (C)&(D) XPS spectrum of MoS_2 nanosheets and S-BN QDs.

3.2 ECL behavior of S-BN QDs

As shown in Fig 2A and B, the PL peak and ECL peak of S-BN QDs were 400 nm and 535 nm, respectively. The significant red shift of the ECL peak from the PL peak was due to the narrower band gaps of QDs surface state (Sun et al., 2009). Fig 2C showed the relation of ECL intensity and excited potential. The excited potential of S-BN QDs was -1.75 V. The cyclic voltammetry was performed with a supporting electrolyte of PBS containing 0.1 mol L^{-1} $K_2S_2O_8$. The wide reduction peak was at -0.72 V (Fig 2D).

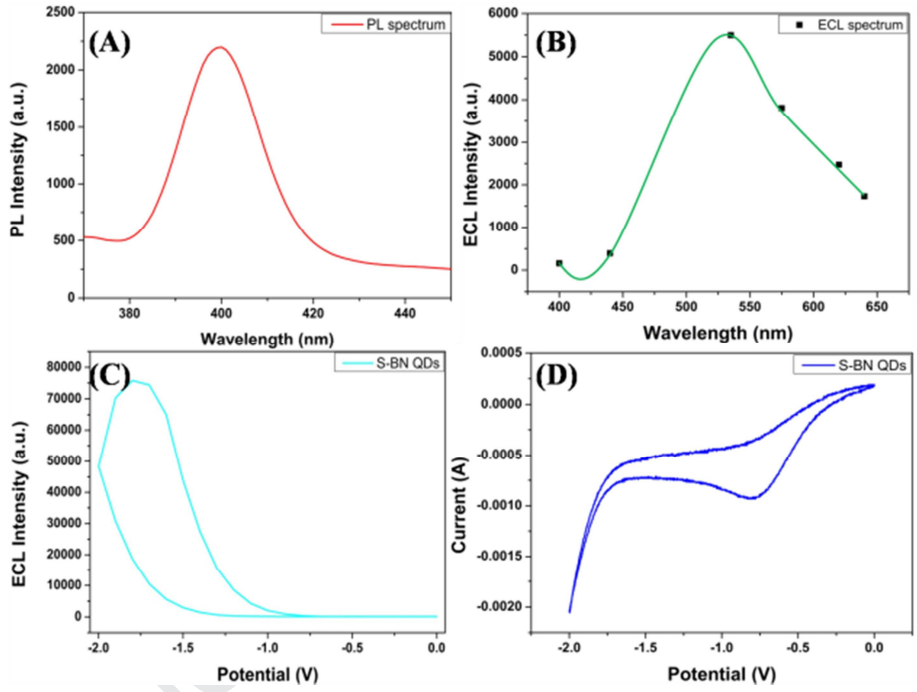

Fig 2. (A) PL spectrum and (B) ECL spectrum of S-BN QDs. (C) Cyclic voltammograms of S-BN QDs/GCE in PBS containing 0.1 mol/L $K_2S_2O_8$. (versus Ag/AgCl reference electrode) (D) ECL behavior of S-BN QDs.

In order to obtain the best ECL intensity of S-BN QDs, the amount of sulfur precursor was optimized (Fig S4). The mechanism of ECL emission was due to the surface defect state of S-BN QDs. The electron transfer process can produce the excited state of QDs. Therefore, more electron transfer on the surface of QDs can enhance the ECL signals. The increase of sulfur led to the decrease of surface defects of S-BN QDs and the more intense electron transfer process on the surface of QDs, which improved the ECL luminous efficiency. So, when the content of sulfur was

equal to the total amount of boron and nitrogen, the ECL signal of S-BN QDs had greatly increased. When the content of sulfur was more than the total amount of boron and nitrogen, excessive sulfur precursor (L-cysteine) was coated on the outside of the QDs, which resulted in the emission site on the surface of the QDs covered. Therefore, ECL luminescence efficiency of the QDs was affected and decreased. The ECL luminescence mechanism of S-BN QDs was the formation of the excited state QDs under the action of free radicals decomposed by $K_2S_2O_8$. The specific ECL luminescence process can be described by the following equations:

$$\text{S-BN QDs} + e^- \rightarrow \text{S-BN QDs}^{\cdot -} \quad (1)$$

$$S_2O_8^{2-} + e^- \rightarrow SO_4^{2-} + SO_4^{\cdot -} \quad (2)$$

$$\text{S-BN QDs}^{\cdot -} + SO_4^{\cdot -} \rightarrow \text{S-BN QDs}^{*} + SO_4^{2-} \quad (3)$$

$$\text{S-BN QDs}^{*} \rightarrow \text{S-BN QDs} + h\nu \quad (4)$$

3.3 The SPC effect of MoS_2 nanosheets

In order to explore the distance-dependent plasmon effect of MoS_2 nanosheets, different lengths of DNA strands were selected to connect MoS_2 nanosheets and S-BN QDs. To avoid the inner filter effect interference of MoS_2 nanosheets, it was assembled on electrode surface. After bound with DNA chain, QDs were connected on the electrode/MoS_2 nanosheet /DNA outside. Then, the effect of the distance between QDs and electrode should be noticed. After the modification of MoS_2 nanosheets on the electrode, there were the joint action of the energy resonance transfer and plasma coupling effect of MoS_2 nanosheets in the ECL process (Fig 3). When S-BN QDs were closed to the surface of MoS_2 nanosheets, the ECL signal of S-BN QDs was completely quenched by the MoS_2 nanosheets. When the distance between S-BN QDs and the MoS_2 nanosheets was 2 nm, the ECL signal of S-BN QDs decreased by 52% due to the ECL energy resonance transfer effect. S-BN QDs worked as ECL energy donor, and MoS_2 nanosheets worked as energy acceptor and ECL quencher. Similarly, when the distance was 5 nm, the ECL signal dropped by 21%. With the increase of distance between MoS_2 nanosheets and S-BN QDs, the

energy transfer effect was limited. And at the same time, the surface plasma coupling effect was strengthened. When the distance increased to ca. 8 nm, the quenching effect from energy transfer and the enhancement from surface plasma coupling were at equilibrium. As a result, the ECL intensity of QDs returned to its original state. When the distance increased by 10 nm, the surface plasma coupling effect of MoS_2 nanosheets had a primary role to play in the ECL amplification, which resulted in the increase of ECL signal by 14%. When the distance was regulated at 12 nm, the ECL intensity increased by 62%. Similarly, when the distance was increased to 15 nm and 19 nm, the ECL signal increased by 96% and 120% respectively. With the increase of distance, surface plasma coupling effect dominated the ECL signal change. It is found that the maximum ECL intensity of QDs reached at a 20 nm distance from MoS_2 nanosheets modified electrode. We also verified this distance-dependent ECL effect by Raman spectroscopy. The Raman signals of MoS_2 nanosheets can be observed in Fig S5. As the distance increased, the energy transfer between QDs and MoS_2 nanosheets was reduced. The recovered strong luminescence signal of QDs caused the decrease of MoS_2 nanosheets Raman signal.

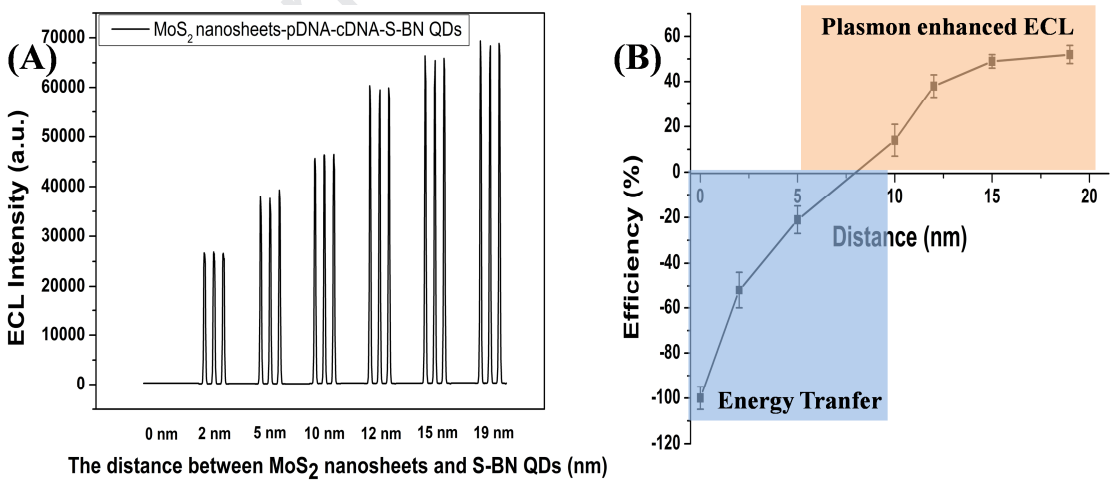

(C)

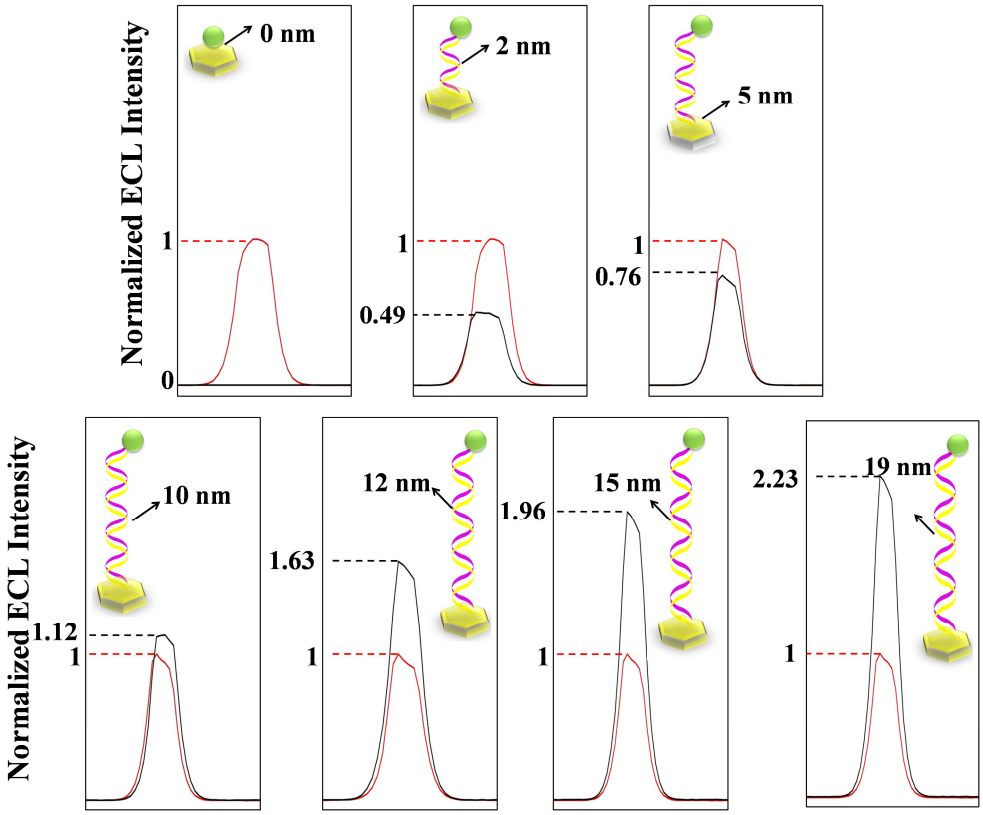

Fig 3 (A) The relation of ECL intensity of the distance between MoS_2 nanosheets and S-BN QDs. (B) The relation of SPC enhanced efficiency and the distance between MoS_2 nanosheets and S-BN QDs. (C) The relation of ECL intensity the distance between GCE and S-BN QDs.

3.4 The SPC-ECL DNA biosensor applications

As shown in Scheme 1, in the plasmon-enhanced ECL-based HCR sensor for HCV gene detection, a mixture of two DNA hairpins (H1 and H2) was compatible and stable in the absence of an initiator (target DNA). The added initiator opened a hairpin (H1) after hybridization in the complementary region, exposing a new single-stranded region capable of opening another hairpin (H2). Then a single-stranded region was produced, which had the same sequence as the target DNA, causing more hairpin DNA (H1) to open. Each initiator can propagate a cascade hybridization event between alternate hairpins to form a long-nicked dsDNA with repeating units. The growth of HCR product did not stop until the hairpin supply was exhausted (Choi et al., 2014). In order to achieve the amplification of the QDs ECL signal, QDs were tagged on H2; MoS_2 nanosheets were connected to H1 on electrodes.

Due to the distance-dependent plasmon coupling effect, the excited QDs near the MoS_2 nanosheets can also undergo resonant interactions and result in ECL enhancement. As is shown in Fig 4A, when MoS_2 nanosheets were decorated on the electrode, the impedance value increased to 132 Ω. After H1 connected with MoS_2 nanosheets, the electron-transfer resistance increased to 425.5 Ω. When target DNA and H2-QDs conjugate connected on the electrode, there was an obvious increase at 730.2 Ω. When the distance between S-BN QDs and MoS_2 nanosheets was 0 nm, the electron-tranfer resistance was 147 Ω; when the distance increased to 19 nm, the impedance result increased to 352 Ω. The ECL intensity of QDs was ca. 27000 in the absence of MoS_2 nanosheets. When MoS_2 nanosheets was introduced the system, the ECL intensity increased to ca. 76000, which increased by 2.8 times (Fig 4B). The binding time of the hairpin DNA were optimized in Fig S6 as 2 hours. Fig 4C displayed the relationship between the concentrations of HCV gene and ECL intensity. The ECL intensity (I) has a linear relationship with logarithm (lg) of HCV gene concentration in the range of 0.5 pM-1 nM (curve a in Fig 4D). The limit of detection (LOD, S/N = 3) was 0.17 pM. To further investigate the reproducibility, intra and inter-assays were performed (Fig S7); the relative standard deviations were 0.64% and 4.51%, respectively, which demonstrated an acceptable repeatability of the proposed biosensor for the detection of HCV gene. To evaluate the specificity of the HCR sensor, the ECL signals of 0.1 nmol target DNA and 0.1 nmol one-base-mismatched DNA were investigated (as shown in Fig S8). Different concentrations of HCV DNA were selected to measure the ECL intensity in human serum. The results were listed in Table S2. The range of recoveries was from 90.00% ~ 105.00% and the RSD was less than 3.13%. The proposed DNA sensor has good accuracy and feasible in the sample.

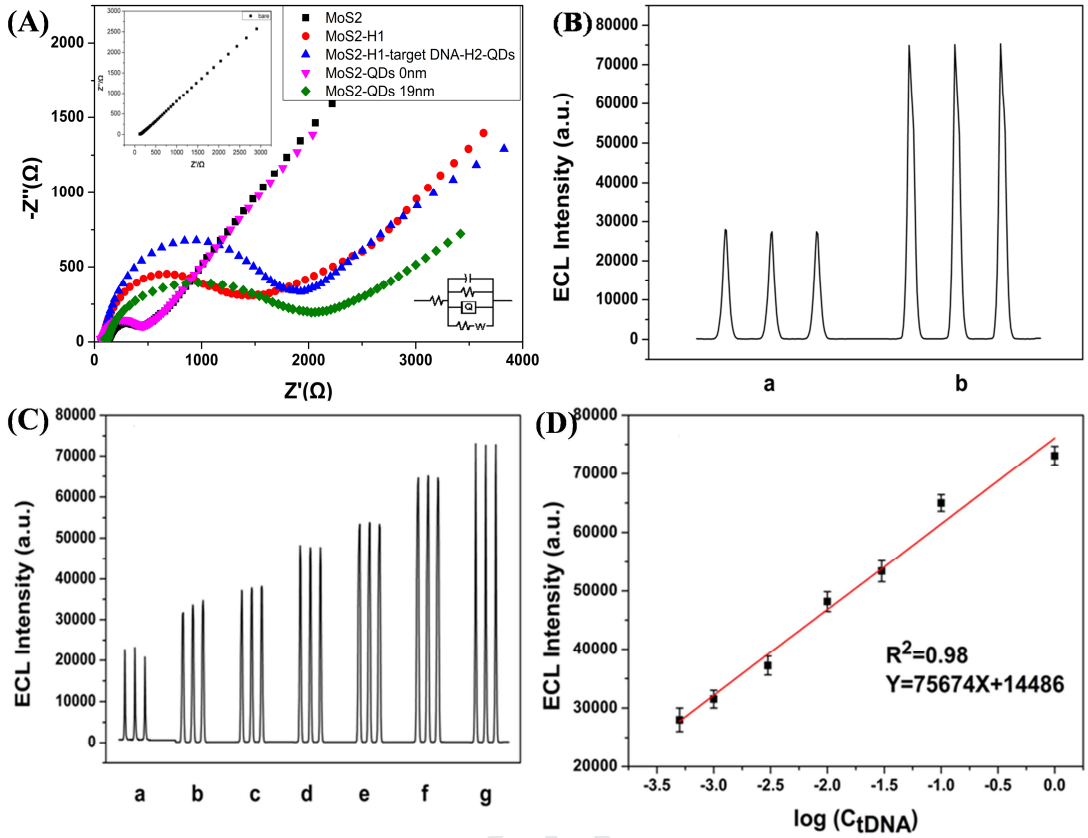

Fig 4 (A) EIS spectrum of different electrodes in 0.1 mol/L KCl solution containing 2.5 mmol/L $K_3[Fe(CN)_6]/K_4[Fe(CN)_6]$. The impedance spectra were recorded in the frequency range of 0.01 Hz to 100 kHz with the amplitude of 5 mV. (B) ECL curves of H1-target DNA-H2-QDs (a) and MoS_2 nanosheets-H1-target DNA-H2-QDs (b). (C) ECL traces of MoS_2 nanosheets-H1-target DNA-H2-QDs of different concentrations of target DNA. (D) Calibration curve for quantification of target DNA.

4. Conclusion

In conclusion, we have synthesized MoS_2 nanosheets as novel nonmetallic plasmonic nanomaterial. In order to explore the plasmon effect of MoS_2 nanosheets, different lengths of DNA strands were employed to regulate the distance between MoS_2 nanosheets and S-BN QDs. With the increase of distance between MoS_2 nanosheets and S-BN QDs, the energy transfer effect was limited and the surface plasma coupling effect was strengthened. The maximum ECL intensity of QDs was observed in the 20 nm distance with MoS_2 nanosheets. Then, an available distance-dependent plasmon enhanced ECL biosensor has been designed successfully.

Based on the hybridization chain reaction amplification, the proposed biosensor can quantify hepatitis C virus. The new sensing mode greatly improved the sensitivity of the sensor and had great potential application in the highly sensitive clinical detection. It should be notice that the surface enhanced ECL effect also has close relationship with the absorption peak of plasmonic materials. So, in order to further improve SPC-ECL sensing performance, the regulation of the absorption peak of plasmonic materials is an important issue to study in the future.

Conflicts of interest

There are no conflicts of interest to declare.

Acknowledgements

The authors gratefully acknowledge financial support from Youth Science Fund of Jilin Province (20140520081JH) and “Thirteenth Five Year” Project of the Science and Technology Research in the Education Department of Jilin Province, China.

References

Alam, R., Labine, M., Karwacki, C. J., Kamat, P. V., 2016. ACS Nano. 10(2), 2880-2886.

Aslan, K., Geddes, C.D., 2009. Chem. Soc. Rev. 38, 2556-2564.

Brody, H., 2011. Nature. 474, S1-S1.

Cheng, H. F., Wen, M. C., Ma, X. C., Kuwahara, Y., Mori, K., Dai, Y., Huang, B. B., Yamashita, H., 2016. J. Am. Chem. Soc. 138(29), 9316-9324.

Choi, H.M.T., Beck, V.A., Pierce, N.A., 2014. ACS Nano. 8(5), 4284-4294.

Deiss, F., LaFratta, C.N., Symer, M., Blicharz, T.M., Sojic, N., Walt, D.R., 2009. J. Am. Chem. Soc. 131(17), 6088-6089.

Delaney, J. L., Hogan, C., Tian, J. F., Shen, W., 2011. Anal. Chem. 83(4), 1300-1306.

Ding, Z. F., Quinn, B. M., Haram, S. K., Pell, L. E., Korgel, B. A., Bard, A. J., 2002.

Science. 296, 1293-1297.

Dirks, R.M., Pierce, N.A., 2004. Proc. Natl. Acad. Sci. USA. 101 (43), 15275-15278.

Ege, D.; Becker, W. G., Bard, A. J., 1984. Anal. Chem. 56(13), 2413-2417.

Eguchi, A., Wree, A., Feldstein, A. E., 2014. J. Hepatol. 60, 1063-1074.

Feng, X. Y., Han, T., Xiong, Y. F., Wang, S.C., Dai, T. Y., Chen, J. H., Zhang, X. J., Wang, G. F., 2019. ACS Sens. 4, 1633-1640.

Gai, Q. Q., Wang, D. W., Huang, R. F., Liang, X. X., Wu, H. L., Tao, X. Y., 2018. Biosens. Bioelectron. 118, 80-87.

Ge,S., Zhao,J., Wang,S., Lan,F., Yan,M., Yu,J., 2018. Biosens.Bioelectron. 102, 411–417.

Halas, N. J., Lal, S., Chang, W. S., Link, S., Nordlander, P., 2011. Chem. Rev. 111, 3913-3961.

Hrift, A. P., EI-Serag, H. B., Kanwal, F., 2007. Nat. Rel. Gastroenterol Hepatol. 14, 122-132.

Huang, Z. F., Song, J. J., Pan, L., Zhang, X. W., Wang, L., Zou, J. J., 2015. Adv. Mater. 27, 5309-5327.

Ishii, S., Shinde, S. L., Nagao, T., 2018. Adv. Opt. Mater. 7(1), 1800603(1-13).

Jiang, J., Ju, J., 2007. Anal. Chem. 79 (17), 6690-6696.

Kaur, B., Sharma, A. K., 2018. Sensing and Imaging. 19, 36(1-6).

Kessentini, S., Barchiesi, D., Andrea, C. D., Toma, A., Guillot, N., Fabrizio, E. D., Fazio, B., Marago, O. M., Gucciardi, P. G., Chapelle, M., 2014. J. Phys. Chem. C. 118, 3209-3219.

Kuwahara, Y., Yoshimura, Y., Haematsu, K., Yamashita, H., 2018. J. Am. Chem. Soc. 140(29), 9203-9210.

Lakowicz, J.R., Ray, K., Chowdhury, M., Szmacinski, H., Fu, Y., Zhang, J.,

Nowaczyk, K., 2008. Analyst. 133, 1308-1346.

Li, L. L., Chen, Y., Zhu, J. J., 2017. Anal. Chem. 89(1), 358-371.

Liu, H. P.; Ye, T.; Mao, C., 2007. Angew. Chem., Int. Ed. 46(34), 6473-6475.

Liu, Y., Chen, X. Q., Wang, M.K., Ma, Q., 2018. Green Chem. 20, 5520-5527.

Liu, Y., Wang, M. K., Nie, Y. X., Zhang, Q., Ma, Q., 2019. Anal. Chem. 91(9), 6250-6258.

Liu, Z. Y., Qi, W. J., Xu, G. B., 2015. Chem. Soc. Rev. 44, 3117-3142.

Long, H., Harley-Trochimczyk, A., Pham, T., Tang, Z. R., Shi, T., Zettl, A., Carraro, C., Worsley, M. A., Maboudian, R., 2016. Adv. Funct. Mater. 26, 5158−5165.

Lou, Z. Z., Gu, Q., Liao, Y. S., Yu, S. J., Xue, C., 2016. Appl. Catal., B. 184. 258-263.

Lou, Z. Z., Gu, Q., Xu, L., Liao, Y. S., Xue, C., 2015. Chem. Asian J. 10(6), 1291-1294.

Lu, H. J., Pan, J. B., Wang, Y. Z., Ji, S. Y., Zhan, W., Luo, X. L., Xu, J. J., Chen, H. Y., 2018. Anal. Chem. 90, 10434-10441.

Miao, W. J., 2008. Chem. Rev. 108, 2506-2553.

Nie,G., Wang,Y., Tang,Y., Zhao,D., Guo,Q., 2018. Biosens. Bioelectron. 101, 123–128.

Peng,L., Yuan,Y., Fu,X., Fu,A., Zhang,P., Chai,Y., Gan,X., Yuan,R., 2019. Anal.Chem. 91, 3239–3245.

Piriaud, F., Russo, L., Pinet, S., Gosse, I., Ravaine, V., Sojic, N., 2013. J. Am. Chem. Soc. 135, 5517-5520.

Qian, G. S., Zhang, T. T., Zhao, W., Xu, J. J., Chen, H. Y., 2017. Chem. Commun. 53, 4710-4713.

Qing, Y., Li, X., Chen, S., Zhou, X. P., Luo, M., Xu, X., Li, C. R., Qiu, J. F., 2017. Microchim Acta. 184, 863-870.

Richter, M., 2004. Chem. Rev. 104, 3003-3036.

Shan, Y., Wu, H. Y., Xiong, S. J., Wu, X. L., Chu, P. K., 2016. Angew. Chem. Int. Ed. 55, 2017-2021.

Shao, L., Woo, K. C., Chen, H., Jin, Z., Wang, J., Lin, H.Q., 2010. ACS Nano. 4, 3053-3062.

Sun, L. F., Bao, L., Hyun, B. R., Bartnik, A. C., Zhong, Y. W., Reed, J. C., Pang, D. W., Abruna, H. D., 2009. Nano Lett. 9(2), 789-793.

Wang, X. L., Ke, Y. J., Pan, H. Y., Ma, K., Xiao, Q. Q., Yin, D. Q., Wu, G., Swihart, M. T., 2015. ACS Catal. 5(4), 2534-2540.

Weinbaum, C. M., Mast, E. E., Ward, J. W., 2009. Hepatology. 49, 35-44.

Wen ,L., Chen, L., Zheng, S. M., Zeng, J. F., Duan, G. X., Wang, Y., Wang, G. L., Chai, Z. F., Li, Z., Gao, M. Y., 2016. Adv. Mater. 28(25), 5072-5079.

Weller, L., Thacker, V. V., Herrmann, L. O., Hemmig, E. A., Lombardi, A., Keyser, U. F., Baumberg, J. J., 2016. ACS Photonics. 3, 1589-1595.

Welzel, T. M., Bhardwaj, N., Hedskog, C., 2017. J. Hepatol. 67, 224-236.

Xie, J. F., Zhang, J. J., Li, S.; Grote, F., Zhang, X. D., Zhang, H., Wang, R. X., Lei, Y., Pan, B. C., Xie, Y., 2013. J. Am. Chem. Soc. 135, 17881−17888.

Xu, Y., Liu, J., Gao, C., Wang, E. K., 2014. Electrochem. Commun. 48 (11), 151-154.

Yu, X. Y., Hu, H., Wang, Y. W., Chen, H. Y., Lou, X. W., 2015. Angew. Chem., Int. Ed. 54, 7395−7398.

Zhang, J., Gryczynski, Z., Lakowicz, J.R., 2004. Chem. Phys. Lett. 393(4-6), 483-487.

Zhu, H., Wang, Y., Chen, C., Ma, M. R., Zeng, J. F., Li, S. Z., Xia, Y. S. Gao, M. Y., 2017. ACS Nano. 11(8), 8273-8281.

Zhu,W., Khan,M.S., Cao,W., Sun,X., Ma,H., Zhang,Y., Wei,Q., 2018. Biosens.

Bioelectron. 99, 346–352.

Captions

Scheme 1. The HCR-based sensing process and distance-dependent plasmon-enhanced ECL

Fig 1. (A)&(B) TEM image of MoS_2 nanosheets and S-BN QDs. (C)&(D) XPS spectrum of MoS_2 nanosheets and S-BN QDs.

Fig 2. (A) PL spectrum and (B) ECL spectrum of S-BN QDs. (C) Cyclic voltammograms of S-BN QDs/GCE in PBS containing 0.1 mol/L $K_2S_2O_8$. (versus Ag/AgCl reference electrode) (D) ECL behavior of S-BN QDs.

Fig 3 (A) The relation of ECL intensity of the distance between MoS_2 nanosheets and S-BN QDs. (B) The relation of SPC enhanced efficiency and the distance between MoS_2 nanosheets and S-BN QDs. (C)The relation of ECL intensity the distance between GCE and S-BN QDs.

Fig 4 (A) EIS spectrum of different electrodes in 0.1 mol/L KCl solution containing 2.5 mmol/L $K_3[Fe(CN)_6]/K_4[Fe(CN)_6]$. The impedance spectra were recorded in the frequency range of 0.01 Hz to 100 kHz with the amplitude of 5 mV. (B) ECL curves of H1-target DNA-H2-QDs (a) and MoS_2 nanosheets-H1-target DNA-H2-QDs (b). (C) ECL traces of MoS_2 nanosheets-H1-target DNA-H2-QDs of different concentrations of target DNA. (D) Calibration curve for quantification of target DNA.

(i) Because MoS_2 nanosheets had obvious optical absorption and scat-tering properties in the visible and near-infrared region, there is a strong resonant coupling between the ECL emission of BN QDs and MoS_2 nanosheets..

(ii) Our results clearly exhibit the distinct distance-dependent effect, with a great ECL enhancement for distance between 12.5 and 20 nm.

(iii) A hybridization chain reaction (HCR) amplification ECL sensing mode with the plasmon-enhanced ECL strategy was constructed.

Credit Author Statement

Liu Yang : Conceptualization; Data curation; Formal analysis;; Investigation; Methodology; Project administration; Resources; Software; Visualization; Writing - original draft; Writing - review & editing.

Nie Yixin: Methodology

Wang Mengke: Methodology

Zhang Qian: Methodology

Ma Qiang: Funding acquisition, Supervision, Validation, Writing - review & editing.

Declaration of interests

☑ The authors declare that they have no known competing financial interests or personal relationships that could have appeared to influence the work reported in this paper.

☐The authors declare the following financial interests/personal relationships which may be considered as potential competing interests: